



HAL
open science

Modeling hydration of mine tailings: Production of hydraulic binders from alkali-activated materials

Philippe Blanc, Adeline Lach, Arnault Lassin, M. Falah, R. Obenaus-Emler,
S. Guignot

► **To cite this version:**

Philippe Blanc, Adeline Lach, Arnault Lassin, M. Falah, R. Obenaus-Emler, et al.. Modeling hydration of mine tailings: Production of hydraulic binders from alkali-activated materials. *Cement and Concrete Research*, 2020, 137, pp.106216 -. 10.1016/j.cemconres.2020.106216 . hal-03492292

HAL Id: hal-03492292

<https://hal.science/hal-03492292>

Submitted on 14 Sep 2022

HAL is a multi-disciplinary open access archive for the deposit and dissemination of scientific research documents, whether they are published or not. The documents may come from teaching and research institutions in France or abroad, or from public or private research centers.

L'archive ouverte pluridisciplinaire **HAL**, est destinée au dépôt et à la diffusion de documents scientifiques de niveau recherche, publiés ou non, émanant des établissements d'enseignement et de recherche français ou étrangers, des laboratoires publics ou privés.



Distributed under a Creative Commons Attribution - NonCommercial 4.0 International License

26 **1. INTRODUCTION**

27 The present paper comes under the general objective of an improved management of waste materials
28 produced during the extraction of valuable minerals from polymetallic sulfidic ores. Beneficiation of
29 such ore bodies starts with the excavation, crushing and comminution of the ore, followed by a pre-
30 sorting step, which depends on the size, the chemical composition or the mineralogical features of the
31 solid materials [1]. The fine materials then undergo a whole chain of enrichment processes to remove
32 the non-valuable or gangue materials, and thus concentrate the metals in a fraction. Most of the
33 separation processes carried out on sulfide minerals are based on froth flotation, a technology by which
34 minerals are mixed in a pulp and are either carried away to a froth phase or kept in the slurry [2],
35 according to their respective and fine-tuned wettability. The comminution stage generates large
36 amounts of sterile waste rock materials, whilst enrichment operations produce tailings or slurries that
37 contain all the unrecovered or less valuable metals and minerals, along with the organic flotation
38 chemicals in process waters [3]. Approximately 14 billion tons of tailings were produced globally by the
39 mining industry in 2010 [4] and this number is on an upward trend as the demand for metals is surging
40 whilst grades in mined ore bodies are declining [5].

41 The environmental impacts associated with mining operations are therefore also growing worldwide.
42 Tailings are frequently disposed of in surface containment facilities, which exposes the materials to
43 weathering [6]. In the case of finely ground sulfide minerals, their high surface area and exposure to air
44 or water lead to increased acid generation and metal mobilization. This contamination can be
45 transferred to the environment through seepages or run-offs of the impoundment. Other potential risks
46 include overburdening and sometimes even disastrous tailings dam breaches, all leading again to
47 uncontrolled releases of detrimental components into the environment. The best available techniques
48 to deal with tailings issues [7] include their storage at the surface as dry stacked materials, or beneath a
49 sufficient depth of water to prevent any reaction with oxygen, as well as their use as thickened paste or

50 backfilling material in the underground cavities resulting from the excavation of the ore. In this case,
51 backfill solutions can be operated with or without a binder.

52 Within the framework of a H2020 project called ITERAMS (Integrated mineral TEchnologies for more
53 sustainable RAw Material Supply), an alternative way of handling the tailings part of mining operations is
54 evaluated [8]. The option studied in the project consists in producing hydraulic binders, and in particular
55 geopolymers, using tailing materials as precursors for the alkali activation reaction. If setting occurs, the
56 resulting material could be used to cover and to isolate the surface-deposited tailings from water
57 infiltration.

58 The case studies of the project include tailings from a Cu/Ni mine located in Northern Europe,
59 investigated as precursors for alkali-activated materials, in a series of previously published experiments
60 [9, 10] which include alkaline leaching, setting and compressive strength tests. The hydration reaction of
61 the tailing materials is composed of two steps. First Si and Al elements are leached out of the tailings,
62 and then these elements combine to form silico-aluminate hydrates. The present study addresses the
63 development of a modeling tool to account for both of these processes, based on the results of the
64 above-mentioned experiments. The model relies on the Pitzer thermodynamic formalism for ion
65 activity, associated with the rate laws for the kinetically controlled dissolutions of primary minerals.
66 Setting up this model requires the selection of reliable values for the thermodynamic properties and the
67 kinetic rate laws, followed by their integration into dedicated databases. Models for setting tests are
68 based on contributions by Roosz et al. [8] for C-S-H ($\text{CaO-SiO}_2\text{-H}_2\text{O}$ hydrates) and M-S-H ($\text{MgO-SiO}_2\text{-H}_2\text{O}$
69 hydrates) solubility, and a solid solution model dedicated to geopolymer precipitation was also
70 specifically developed in the present work. The whole modeling process was tested and is in good
71 agreement with the results of the compressive tests.

72 **2. DATABASE DEVELOPMENTS**

73 Alkali activation involves interactions with high ionic strength solutions. We considered as a starting
74 point the Thermoddem thermodynamic database [11], which provides a large set of minerals and
75 includes the temperature dependence for most of the thermodynamic functions. The database was
76 expanded to take into account the main aqueous species at high pH, by considering the Pitzer model for
77 high electrolyte concentrations and the corresponding interaction coefficients between them.
78 Interaction parameters collected by Plummer et al. [12] were incorporated into the database.
79 Interaction parameters for the main ions of the systems were specifically reviewed, as explained below.
80 Aqueous complexes were removed when their formation could interfere with ion interactions in the
81 Pitzer formalism. The consistency of the resulting database was checked by comparing the calculation
82 results with the experimental solubilities for several minerals of interest in the alkaline systems. During
83 contact with alkali solution, minerals and especially silicates, progressively dissolve in accordance with
84 their respective kinetic rate laws. To take into account the main minerals forming the tailing materials,
85 we completed the kinetic database [13], distributed along with Thermoddem, for dissolution rate laws in
86 high pH solutions.

87 The final goal of the study is to produce a modeling tool capable of assessing the setting potential of a
88 given mine tailing material. Setting occurs when the precipitating silicate hydrates with hydraulic binder
89 properties like C-S-H and M-S-H. For such phases, the model proposed by Roosz et al. [14] was used.
90 Mine tailing activation could also produce geopolymers, of which the silicate structure is closer to that
91 of zeolites. To account for this second potential precipitation path, a specific solid solution model was
92 developed, based on the thermodynamic properties of zeolites of low crystallinity.

93 **2.1. Thermodynamic relations**

94 We consider the equilibrium of a solid AB in an aqueous solution with the dissolved species A^+ and B^- :



96 where the equilibrium constant of the reaction, $(K_{AB})_{P,T}$, is related to the Gibbs free energy of the
 97 reaction $(\Delta_r G^0_{AB})_{P,T}$ by:

98
$$\text{Log}K_{AB,P,T} = -\frac{\Delta_r G^0_{AB,P,T}}{R \cdot T \cdot \ln(10)}$$
 (2)

99 where R and T stand for the ideal gas constant and the temperature, respectively. The relation between
 100 the Gibbs free energy of reaction and of formation, for each reaction component AB, A⁺ and B⁻, is given
 101 by:

102
$$\Delta_r G^0_{AB,P,T} = \Delta_f G^0_{A^+,P,T} + \Delta_f G^0_{B^-,P,T} - \Delta_f G^0_{AB,P,T}$$
 (3)

103 $\Delta_f G^0_{AB,P,T}$ is related to its first and second derivatives (enthalpy $\Delta_f H^0_{AB,P,T}$, entropy $\Delta_f S^0_{AB,P,T}$ and heat
 104 capacity $C_{p,AB}$) with respect to temperature and pressure through:

105
$$\Delta_f G^0_{AB,P,T} = \Delta_f H^0_{AB,P,T} - T \cdot \Delta_f S^0_{AB,P,T}$$

 106
$$= \Delta_f H^0_{AB,Pr,Tr} - T \cdot \Delta_f S^0_{AB,Pr,Tr} + \int_{Tr}^T C_{p,AB} dT - T \cdot \int_{Tr}^T \frac{C_{p,AB}}{T} dT + \int_{Pr}^P V_{AB} dP$$
 (4)

107 where Pr (0.1 MPa) and Tr (298.15 K) are the reference pressure and temperature and V_{AB} is the molar
 108 volume of AB (in $\text{cm}^3 \cdot \text{mol}^{-1}$).

109 Finally, the third law entropy necessary for calculating apparent standard properties of any compound
 110 at any temperature T is calculated by subtracting the entropy of the elements from the formation
 111 entropy. In this work, a solid solution model was developed for geopolymers and used in a geochemical
 112 code, which supposes that the database is provided with LogK(T) functions for each end-member. In this
 113 work, end-member LogK(T) functions are calculated from formation properties, estimated using a
 114 polyhedral decomposition model, as described in the following sections.

115 **2.2. Description of solute activity coefficients**

116 The Thermoddem database relies on the detailed description of the existing aqueous complexes or, at
117 least, of those identified in the literature. It is used, by default, with the extended Debye-Hückel model
118 for activity coefficients, which depend on the ionic strength of the aqueous solutions only, however, the
119 corresponding range of application is ionic strength-limited.

120 On the other hand, the Pitzer approach [15-20] was developed to describe highly concentrated systems
121 and its validity range is limited by the solubility of salt minerals [21, 22]. Details are given in Appendix A,
122 together with a description of the different parameters involved. It relies on the use of specific
123 interaction parameters and preferentially considers fully dissociated electrolytes. However, it is still
124 possible to consider ion pairing with the Pitzer model by including the formation of aqueous complexes
125 [21-24]. In addition, the Pitzer equations for activity coefficients also include a Debye-Hückel term that
126 depends on ionic strength. Therefore, there is room to propose a modeling strategy that consistently
127 merges the two approaches: strong major electrolytes (Table 1) are described according to the Pitzer
128 formalism, with limited ion pairing, while aqueous complexation reactions are considered for
129 compounds that contain minor or trace elements. This database building strategy depends on the
130 chemical system of interest, in our case it applies to alkaline pH conditions, with Na-dominated
131 solutions.

132 Considering the Thermoddem database [11] and interaction parameters from Plummer et al. [12] as a
133 starting point, a focus was put on refining the collection of interaction parameters for the main ions in
134 our system. The refined collection considers the hydroxylated form of the dissolved elements, as
135 expected in alkaline media. The references used for the refined collection are reported in Table 1 and
136 the parameter values are given in Table 2 for binary and in Table 3 for ternary interactions. The
137 database is developed for use with the PHREEQC software [25], therefore, the interaction parameters
138 depend on the temperature according to the following equation:

$$Y(T) = A_0 + A_1 \left(\frac{1}{T} - \frac{1}{T_r} \right) + A_2 \ln \left(\frac{T}{T_r} \right) + A_3 (T - T_r) + A_4 (T^2 - T_r^2) + A_5 \left(\frac{1}{T^2} - \frac{1}{T_r^2} \right) \quad (5)$$

139 where Y(T) stands for any interaction parameter listed in Table 2 and Table 3; T and T_r correspond to the
 140 temperature (in K) and the reference temperature (298.15 K), respectively; A₀ to A₅ represent empirical
 141 coefficients. The coefficients listed in Table 2 and Table 3 were collected from the references cited, then
 142 put into consistency with equation (5). When no value could be found for interaction parameters in
 143 alkaline solutions, the value was set to 0.

144 Table 1. References for the collected Pitzer interaction parameters

	OH ⁻	Al(OH) ₄ ⁻	Fe(OH) ₄ ⁻	Fe(OH) ₃ ⁻	H ₂ SiO ₄ ⁻²
Na ⁺	(1)	(4)	--	--	(5)
K ⁺	(2)	(4)	--	--	--
Ca ⁺²	(3)	--	--	--	--
Mg ⁺²	--	--	--	--	--

145 (1) Lach [26]. The parameterization is valid up to saturation between 0 and 150°C. For this, partial dissociation is
 146 considered and the neutral species NaOH⁰(aq) is introduced.

147 (2) Christov and Moller [27]. The parameterization is valid up to 5 mol·kg⁻¹ between 0 and 170°C.

148 (3) Christov and Moller [28].

149 (4) Wesolowski and Palmer [29]. The interaction parameters can be determined from the interaction parameters
 150 of Na-OH and K-OH, following these equations:

$$\left(\beta^{(0)}(Na^+/OH^-) - \beta^{(0)}(Na^+/Al(OH)_4^-) \right) = \left(\beta^{(0)}(K^+/OH^-) - \beta^{(0)}(K^+/Al(OH)_4^-) \right) = 0.0356 \quad (6)$$

$$\left(\beta^{(1)}(Na^+/OH^-) - \beta^{(1)}(Na^+/Al(OH)_4^-) \right) = \left(\beta^{(1)}(K^+/OH^-) - \beta^{(1)}(K^+/Al(OH)_4^-) \right) = 0 \quad (7)$$

$$\left(C^\phi(Na^+/OH^-) - C^\phi(Na^+/Al(OH)_4^-) \right) = \left(C^\phi(K^+/OH^-) - C^\phi(K^+/Al(OH)_4^-) \right) = 0.00526 \quad (8)$$

151 (5) Felmy, Cho, Rustad and Mason [30]. In theory, valid between 22 and 25°C. In this paper, the authors provide
 152 interaction parameters for other silica species (H₃SiO₄⁻; Si₂O₂(OH)₅⁻; Si₂O₃(OH)₄⁻²; Si₃O₆(OH)₃⁻³; Si₃O₅(OH)₅⁻³;
 153 (Si₄O₈)(OH)₄⁻⁴; Si₄O₆(OH)₆⁻²; Si₄O₇(OH)₆⁻⁴; Si₆O₁₅⁻⁶)
 154

155 Verification calculations were carried out, based on mineral solubility in high ionic strength solutions.

156 The results are reported in Fig. 1 which displays:

157 - Gibbsite solubility vs. NaOH concentration in aqueous solutions between 25 and 90°C

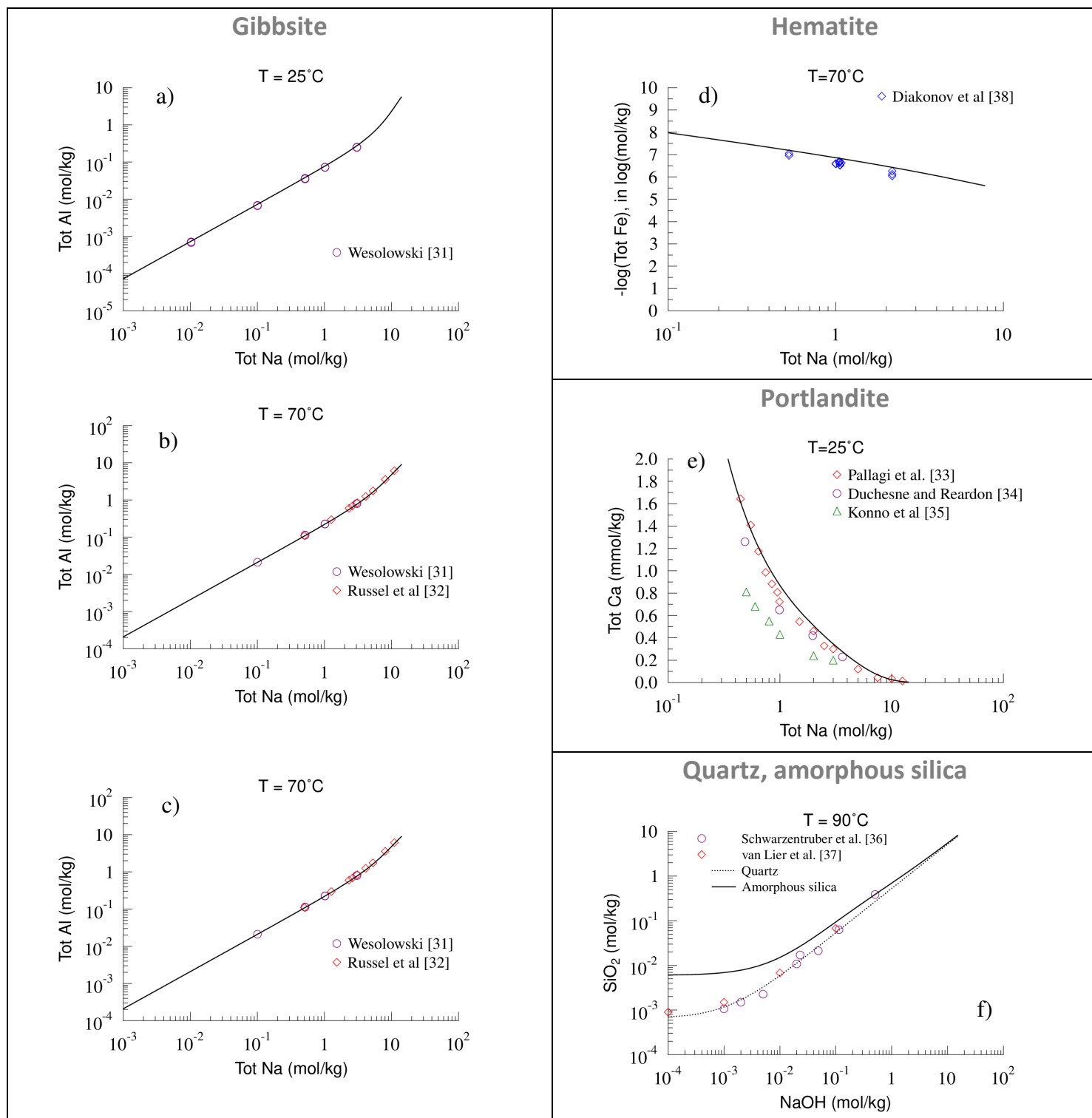
158 - Portlandite solubility vs. NaOH concentration in aqueous solutions at 25°C, similar results are
 159 obtained for KOH solutions

160 - Silica solubility vs. NaOH concentration in aqueous solutions at 90°C

161 - Hematite solubility vs. NaOH concentration in aqueous solutions at 70°C.

162 In Fig. 1.f, experimental points correspond to the solubility of quartz obtained by Van Lier et al. [36] and
163 Schwarzenhuber et al. [37]. The calculated solubility of amorphous silica is also displayed for
164 comparison purpose with quartz solubility. Globally, the calculation results displayed in Fig. 1 show good
165 overall agreement with the data from the literature, given the scattering of the datasets that could be
166 gathered.

167



168 Figure 1. Pitzer interaction parameter verification against solubility data from the literature [31-38].
 169 Reported concentrations correspond to the total amounts of the dissolved elements. Solubility of
 170 gibbsite $\text{Al}(\text{OH})_3$ across varying NaOH concentrations at a) 25°C [31], b) 70°C [31, 32] and c) 90°C [32]; d)
 171 solubility of Hematite Fe_2O_3 [38]; e) solubility of portlandite $\text{Ca}(\text{OH})_2$ at 25°C [33-35]; f) solubility of SiO_2
 172 at 90°C [36-37].

Table 2. Coefficients for the temperature dependence of Pitzer binary interaction parameters (eq. (5))

System	Parameter	A_0	A_1	A_2	A_3	A_4	A_5
Na-OH	$\beta^{(0)}(Na^+/OH^-)$	9.865E-02	-1.741E+03	-1.160E+01	2.768E-02	-1.138E-05	2.060E+04
	$\beta^{(1)}(Na^+/OH^-)$	1.941E-01	2.139E+04	9.166E+01	-1.812E-01	6.407E-05	-1.072E+06
	$C^\phi(Na^+/OH^-)$	2.528E-03	3.201E+02	1.618E+00	-3.436E-03	1.324E-06	-1.011E+04
	$\zeta(Na^+/OH^-/NaOH_{aq}^0)$	1.280E-03	-1.427E+01	-1.827E-01	6.060E-04	-3.014E-07	3.827E-02
	$\lambda(NaOH_{aq}^0/NaOH_{aq}^0)$	2.068E-02	4.070E+02	3.372E+00	-9.666E-03	4.500E-06	1.445E-01
Na-Al(OH) ₄	$\beta^{(0)}(Na^+/Al(OH)_4^-)$	6.295E-02	-1.970E+03	-1.254E+01	2.938E-02	-1.195E-05	3.089E+04
	$\beta^{(1)}(Na^+/Al(OH)_4^-)$	1.941E-01	2.139E+04	9.166E+01	-1.812E-01	6.407E-05	-1.072E+06
	$C^\phi(Na^+/Al(OH)_4^-)$	-2.730E-03	3.253E+02	1.640E+00	-3.475E-03	1.337E-06	-1.035E+04
K-OH	$\beta^{(0)}(K^+/OH^-)$	1.373E-01	1.465E+02	-2.277E-03	7.922E-04	-1.488E-09	2.328E+01
	$\beta^{(1)}(K^+/OH^-)$	3.349E-01	-2.162E+03	-4.825E-02	-1.704E-02	-3.318E-08	4.690E+02
	$C^\phi(K^+/OH^-)$	1.789E-03	-2.233E+01	-5.894E-05	-2.021E-04	-5.274E-11	2.695E-01
K-Al(OH) ₄	$\beta^{(0)}(K^+/Al(OH)_4^-)$	1.017E-01	1.470E+02	-4.903E-05	7.880E-04	-2.549E-11	6.340E-01
	$\beta^{(1)}(K^+/Al(OH)_4^-)$	3.349E-01	-2.162E+03	-4.825E-02	-1.704E-02	-3.318E-08	4.690E+02
	$C^\phi(K^+/Al(OH)_4^-)$	-3.471E-03	-2.233E+01	-5.691E-05	-2.021E-04	-5.019E-11	2.630E-01
Ca-(OH) ₂	$\beta^{(0)}(Ca^{+2}/OH^-)$	-1.098E-01	4.152E+02	2.576E-04	2.636E-04	1.635E-10	-2.623E+00
	$\beta^{(1)}(Ca^{+2}/OH^-)$	-2.303E-01	0.0	0.0	0.0	0.0	0.0
	$\beta^{(2)}(Ca^{+2}/OH^-)$	-5.720E+00	0.0	0.0	0.0	0.0	0.0
Na-H ₂ SiO ₄ ²⁻	$\beta^{(0)}(Na^+/H_2SiO_4^{2-})$	3.200E-01	0.0	0.0	0.0	0.0	0.0
	$\beta^{(1)}(Na^+/H_2SiO_4^{2-})$	1.300E-01	0.0	0.0	0.0	0.0	0.0

175

176

177

178

179

180

181

Table 3. Coefficients for the temperature dependence of Pitzer ternary interaction parameters (eq. (1))

Parameter	A_0	A_1	A_2	A_3	A_4	A_5	References
$\theta(\text{Na}^+/\text{K}^+)$	$-3.203 \cdot 10^{-3}$	$1.402 \cdot 10^1$	$-7.370 \cdot 10^{-6}$	$1.414 \cdot 10^{-8}$	$-5.053 \cdot 10^{-12}$	$7.228 \cdot 10^{-2}$	[39]
$\theta(\text{Na}^+/\text{Ca}^{+2})$	$5.00 \cdot 10^{-2}$	0.0	0.0	0.0	0.0	0.0	[40]
$\theta(\text{Na}^+/\text{Mg}^{+2})$	$7.00 \cdot 10^{-2}$	0.0	0.0	0.0	0.0	0.0	[41]
$\theta(\text{K}^+/\text{Ca}^{+2})$	$1.16 \cdot 10^{-1}$	0.0	0.0	0.0	0.0	0.0	[41]
$\theta(\text{OH}^-/\text{Al}(\text{OH})_4^-)$	$1.40 \cdot 10^{-2}$	0.0	0.0	0.0	0.0	0.0	[31]
$\psi(\text{Na}^+/\text{OH}^-/\text{Al}(\text{OH})_4^-)$	$-4.80 \cdot 10^{-3}$	0.0	0.0	0.0	0.0	0.0	[31]
$\psi(\text{Na}^+/\text{OH}^-/\text{Al}(\text{OH})_4^-)$	$-4.80 \cdot 10^{-3}$	0.0	0.0	0.0	0.0	0.0	[31]

182

183

184

Table 4. Dissolution rate law parameters refined in this study.

	$\log k_{\text{H}^+}$ $\log (\text{mol} \cdot \text{m}^{-2} \cdot \text{s}^{-1})$	$\log k_{\text{nu}}$ $\log (\text{mol} \cdot \text{m}^{-2} \cdot \text{s}^{-1})$	$\log k_{\text{OH}^-}$ $\log (\text{mol} \cdot \text{m}^{-2} \cdot \text{s}^{-1})$	E_{H^+} $\text{kJ} \cdot \text{mol}^{-1}$	E_{nu} $\text{kJ} \cdot \text{mol}^{-1}$	E_{OH^-} $\text{kJ} \cdot \text{mol}^{-1}$	n_{H^+}	n_{OH^-}
Anorthite	-5.66	-11.59	-7.67	62584	62584	62584	1.10	0.58
Actinolite/Hornblende	-10.52	-20.00	-10.94	52716	52716	52716	0.34	0.19
Tremolite	-10.88	-12.79	-10.47	52716	52716	52716	0.37	0.29
Diopside	-9.86	-18.26	-10.75	44815	44815	44815	0.16	0.17
Forsterite	-6.91	-10.44	--	62382	62382	--	0.44	--
Enstatite	-9.34	-11.90	-10.76	63692	63692	63692	0.29	0.81

185

186

187

188

189

Table 5. Polyhedral decomposition matrix for geopolymer Gibbs free energy assessment

		CaO	Na ₂ O	Al ₂ O ₃	SiO ₂	H ₂ O	$\Delta_f G^0$ obs. kJ.mol ⁻¹	$\Delta_f G^0$ calc. kJ.mol ⁻¹	Δ kJ.mol ⁻¹	References
Lime	CaO	1.00					-603.30	-603.30	0.00	[11]
SiO ₂ (am)	SiO ₂				1.00		-856.28	-852.49	3.79	[11]
Mordenite	Ca _{0.515} Al _{1.03} Si _{4.97} O ₁₂ ·3.1H ₂ O	0.515		0.515	4.970	3.100	-6176.95	-6177.64	0.69	[42]
Analcime	Na _{0.99} Al _{0.99} Si _{2.01} O ₆ ·H ₂ O	0.000	0.495	0.495	2.010	1.000	-3089.00	-3071.17	-17.83	[42]
Natrolite	Na ₂ Al ₂ Si ₃ O ₁₀ ·2H ₂ O	0.00	1.00	1.00	3.00	2.00	-5316.60	-5295.44	-21.16	[42]
Clinoptilolite	Ca _{0.55} (Si _{4.9} Al _{1.1})O ₁₂ ·3.9H ₂ O	0.55	0.00	0.55	4.90	3.90	-6390.27	-6389.62	-0.65	[42]
Zeolite X	Na ₂ Al ₂ Si _{2.5} O ₉ ·6.2H ₂ O		1.00	1.00	2.50	6.20	-5847.50	-5865.18	17.68	[43]
Zeolite Y	Na ₂ Al ₂ Si ₄ O ₁₂ ·8H ₂ O		1.00	1.00	4.00	8.00	-7552.50	-7570.76	18.26	[43]
Merlinoite	Na _{1.04} Al _{1.04} Si _{1.96} O ₆ ·2.27H ₂ O	0.00	0.52	0.52	1.96	2.27	-3389.00	-3386.30	-2.70	[42]
Zeolite A (am)	NaAlSiO ₄ ·2.25H ₂ O	0.00	0.50	0.50	1.00	2.25	-2527.00	-2517.90	-9.10	[44]
End member 1	NaSiAlO ₄ ·2.25H ₂ O	0.00	0.50	0.50	1.00	2.25		-2517.90		
End member 2	Na _{0.4} Si _{1.6} Al _{0.4} O ₄ ·2.25H ₂ O	0.00	0.20	0.20	1.60	2.25		-2350.28		
$\Delta_f G^0$ (kJ.mol ⁻¹)		-603.30	-525.92	-1737.78	-852.49	-237.14				

192 2.3. Kinetic rates database

193 The kinetic part of the database, which includes dissolution and precipitation rates, is based on the
194 compilation proposed by Marty et al. [13]. For the present study, it has been supplemented with
195 several minerals, extracting the dissolution rate in high pH solutions. In the Marty et al. [13]
196 compilation, the rate law corresponds to a formalism proposed by Lasaga et al. [45], where the
197 dissolution rate coefficient k (in $\text{mol}\cdot\text{m}^{-2}\cdot\text{s}^{-1}$) is given by:

$$198 \quad k = k^0 \cdot A_{\text{min}} \cdot e^{-\frac{E_A}{R \cdot T}} \cdot a_{\text{H}^+}^{n_{\text{H}^+}} \cdot \prod_i a_i^{n_i} \cdot f(\Delta_r G) \quad (9)$$

199 with:

200 k^0 : kinetic constant ($\text{mol}\cdot\text{m}^{-2}\cdot\text{s}^{-1}$)

201 A_{min} : surface area of the mineral ($\text{m}^2\cdot\text{g}^{-1}$)

202 E_A : activation energy of the overall reaction ($\text{J}\cdot\text{mol}^{-1}$)

203 R : gas constant ($8.314 \text{ J}\cdot\text{mol}^{-1}\cdot\text{K}^{-1}$)

204 T : absolute temperature (K)

205 a_i and a_{H^+} : activities in solution of species i and H^+ , respectively

206 n_i and n_{H^+} : orders of the reaction with respect to these species

207 $f(\Delta_r G)$: thermodynamic term of the kinetic law which is a function the Gibbs free energy of the
208 overall reaction ($\text{J}\cdot\text{mol}^{-1}$)

209

210 Equation (9) is divided into three domains, depending on the pH range. It applies strictly to the acidic
211 domains. For neutral conditions, $a_{\text{H}^+}^{n_{\text{H}^+}} = 1$. In the basic domain, the $a_{\text{H}^+}^{n_{\text{H}^+}}$ is replaced by $a_{\text{H}^+}^{n_{\text{OH}^-}}$. For
212 each domain, a set of k^0 , E_a and n_i values is extracted from a compilation of literature data. The
213 results are illustrated in Fig. B1 to B6, Appendix B, for 6 minerals and the parameters extracted from

214 literature data are reported in Table 4. The 6 dissolution rate laws are implemented in the kinetic
215 database.

216 **2.4. Geopolymer solid solution**

217 The structure, chemical composition and properties of geopolymers have been reported for decades
218 by various authors. Davidovits [46] and Provis [47] give comprehensive summaries of their properties
219 and uses. Duxson et al. [48], [49], Provis and Van Deventer [50] and Provis and Bernal [51] dedicated
220 several studies to refining their structure and describing their mechanisms of formation. As for
221 hydraulic binders produced from alkali-activated processes, Luukkonen et al. [52] summarized a
222 debate about terminology, indicating that binders prepared from alkali activation could contain more
223 Q^2 silicon tetrahedra than geopolymers, which are essentially based on a three-dimensional
224 structure, close to zeolites, and richer in Q^4 coordinated tetrahedra. However, the terms
225 “geopolymers” and “alkali-activated materials” are used alternatively in the literature, and often as
226 synonyms, which can lead to misunderstandings. In the present study, we completed the modeling of
227 alkali activation with an ideal solid solution geopolymer model, which allows the presence of this
228 phase in the reaction products, among other hydraulic binders, to be discussed.

229 In order to consider a geopolymer in a solid solution model, chemical formulas for its end members
230 must be provided. In this regard, we rely on the formula given by Xiong [44] for the amorphous
231 zeolite A, $NaAlSiO_4 \cdot 2.25H_2O$. Provis et al. [50] indicate that maximum compressive resistances are
232 obtained for compositions displaying $Si/Al = 2$. Therefore, a binary solid solution should bracket such
233 a composition, which is achieved by choosing a composition of end-members in which $Si/Al = 1$ and
234 $Si/Al = 4$, giving the following molar formula: $NaAlSiO_4 \cdot 2.25H_2O$ and $Na_{0.4}(Al_{0.4}Si_{1.6})O_4 \cdot 2.25H_2O$.

235 To determine the thermodynamic properties ($\Delta_f G^0$, S^0 and C_p^0) of both end members, a polyhedral
236 decomposition model was developed, which consists in decomposing the chemical formula of a given
237 mineral into basic units of known thermodynamic properties, in order to calculate those for the

238 mineral of interest. The method had been extensively used in previous literature and especially
 239 detailed by Hazen [53] and Chermak and Rimstidt [54]. The properties of the basic units are refined
 240 from a set of minerals of known properties, as proposed by Blanc et al. [42].

241

242 Table 6. Results of polyhedral decomposition for geopolymer entropy S^0 and heat capacity C_p^0
 243 assessment

	S° obs J.mol ⁻¹ .K ⁻¹	S° calc. J.mol ⁻¹ .K ⁻¹	Δ J.mol ⁻¹ .K ⁻¹	C_p° obs. J.mol ⁻¹ .K ⁻¹	C_p° calc. J.mol ⁻¹ .K ⁻¹	Δ J.mol ⁻¹ .K ⁻¹	References
Lime	38.10	38.10	0.00	42.05	42.05	0.00	[11]
SiO ₂ (am)	41.44	52.60	-11.16	59.89	52.31	7.58	[11]
Mordenite	470.57	464.18	6.39	443.11	441.54	1.57	[42]
Analcime	231.10	212.24	18.86	212.38	211.59	0.79	[42]
Natrolite	359.73	371.92	-12.19	359.23	370.87	-11.64	[42]
Clinoptilolite	498.89	504.88	-5.99	481.02	482.49	-1.47	[42]
Zeolite X	566.00	563.72	2.28	586.00	574.73	11.27	[43]
Zeolite Y	734.00	736.09	-2.09	739.00	751.77	-12.77	[43]
Merlinoite	283.43	278.31	5.12	305.68	281.14	24.54	[42]
End member 1		224.57			227.74		
End member 2		223.05			227.80		

244

245 Table 7. Thermodynamic properties refined for polyhedral basic units

	CaO	Na ₂ O	Al ₂ O ₃	SiO ₂	H ₂ O
$\Delta_f G^{\circ}$ (kJ.mol ⁻¹)	-603.30	-525.92	-1737.78	-852.49	-237.14
S° (J.mol ⁻¹ .K ⁻¹)	38.10	67.24	43.03	52.60	51.93
C_p° (J.mol ⁻¹ .K ⁻¹)	42.05	123.56	-19.14	52.31	54.77

246

247 The observed thermodynamic properties were selected based on the publications of Blanc et al. [11],
 248 Blanc et al. [42], Lothenbach et al. [43] and Xiong [44]. The two latter correspond to low crystallinity
 249 zeolites. Table 5 gives the decomposition matrix and the results for the Gibbs free energy. In this
 250 case, $\Delta_f G^{\circ}$ of the H₂O component is constrained to prevent it from exceeding the $\Delta_f G^{\circ}$ of bulk water.
 251 Table 6 presents the results for entropy and heat capacity at room temperature. In this case, the
 252 entropy provided by Xiong [44] for zeolite A, 648 J.mol⁻¹.K⁻¹, could not be selected for S° refinement,
 253 because its value is completely different from the entropy calculated using polyhedral basic units
 254 refined here, 225.40 J.mol⁻¹.K⁻¹. Furthermore, the Helgeson estimate method [55] provides 233

255 J.mol⁻¹.K⁻¹ for Zeolite A, which is quite close to the value calculated here. The entropy extracted by
256 Xiong [44] is considered as an outlier and is not used here. Finally, the properties of polyhedral basic
257 units, refined by minimizing the sum of square differences between calculated and observed values,
258 are given in Table 7. For each geopolymer end-member 1 and 2, the thermodynamic properties are
259 reported in Table 5 and Table 6. The resulting set of thermodynamic properties, for the respective
260 NaAlSiO₄·2.25H₂O and Na_{0.4}(Al_{0.4}Si_{1.6})O₄·2.25H₂O end members, corresponds respectively to:

261 - $\Delta G_f^\circ = -2517.90$ and -2350.28 kJ.mol⁻¹

262 - $S^\circ = 224.57$ and 227.74 J.mol⁻¹.K⁻¹

263 - $C_p^\circ = 223.05$ and 227.80 J.mol⁻¹.K⁻¹.

264

265

266

267

268 3. LEACHING AND SETTING EXPERIMENTS

269 Previous developments were then tested by modeling the results of the experiment tests. These
270 results are fully described in companion papers (Obenaus-Emler et al. [10] and Falah et al. [9]) and
271 thus, only a short description of the experiment design and of the results is given here.

272 Mine tailing samples were collected from a Cu/Ni mine located in Northern Europe. Samples were
273 ground using ball mill [10] or disc mill [9], bringing the mean diameter of particles to 7.5 and 4.0 μm ,
274 respectively. Particle size distributions were measured by laser diffraction. Additionally, mine tailings
275 were characterized by XRD. In the present study, Rietveld refinement was carried out at BRGM using
276 the BGMN/PROFEX software [56]. The results are reported in Table 8. The mineralogy appears to be
277 dominated by mafic minerals such as amphiboles (tremolite, actinolite), pyroxenes (diopside,
278 enstatite) or feldspars, including additional phyllosilicates (biotite, chlorite). The analysis was also
279 performed on hardened samples, after setting and compressive strength tests. No new crystalline
280 phase could be detected, even using Rietveld refinement, which is not surprising since hydraulic
281 binders are amorphous or near-amorphous phases. However, this also prevents the relative amounts
282 of possibly produced C-S-H, M-S-H or geopolymer phases from being determined.

283 Leaching tests were carried out in similar conditions for both groups of authors:

284 - Falah et al. [9]: dissolution was performed by mixing 0.5 g of sample with 20 g of 6M NaOH solution,
285 for 24h at $23 \pm 0.5^\circ\text{C}$. After filtration and acidification, the solutions were analyzed for their dissolved
286 Si and Al content by ICP-OES.

287 - Obenaus-Emler et al. [10]: dissolution was performed by pouring 2 g of sample into 100 ml of
288 solvent (5M and 10M NaOH) and leaving the solid to react for 72 hours at 40°C . After 3 days, samples
289 were filtered and acidified prior to determining the amount of dissolved species by ICP-MS.

290 Using the same initial tailing material as for leaching tests, hardening experiments were performed
291 by both groups of authors. The mixing and curing conditions were quite similar, with Na_2SiO_3 solution
292 used as an activator. The investigated parameters are the concentration of the activator solvent [9]
293 and the curing temperature [10], according to the following short description:

294 - Falah et al. [9]: various concentrations of the activator were considered, from 10 to 30% Na_2SiO_3 .
295 Only extreme 10 and 30% concentrations were selected here to compare with modeling calculations.
296 The liquid to solid ratio is set at 0.23. Hardened samples were cured for 7, 14 and 28 days at 40°C.

297 - Obenaus-Emler et al. [10]: suspensions were prepared with 100 g of ground mine tailing sample and
298 27.5 ml of activator solution (Na_2SiO_3 30%). Hardened samples were then cured for 7, 14 and 28 days
299 at 40°C and 60°C.

300 For both groups of authors, XRD analysis failed to identify the precipitation of hydraulic binders in
301 the hardened materials, most likely due to their gel-like structure. Still, Falah et al. [9] performed
302 SEM-EDX (Scanning Electron Microscope with Energy Dispersive X-Ray Analyzer) observations and
303 analyses. For a sample activated with Na_2SiO_3 30% at 40°C for 28 days, they observed reticulated
304 microstructure around residual clumps of initial tailing materials. Flaky structures became more
305 obvious as the concentration in Na_2SiO_3 increased, revealing the appearance of binder phases, the
306 composition of which could not be precisely determined by SEM-EDX.

307 **4. MODEL AND SPECIFIC INTERFACE DEVELOPMENT**

308 Based on the Thermoddem [11] database (Table D1 in Appendix D), Pitzer interaction terms are
309 included and kinetic rates of mineral dissolution (Table 4) are added as reported previously.
310 Geochemical modeling of both the alkaline leaching and the setting under alkaline activation is
311 carried out. The aim is to reproduce previously described experiments, to provide a tool able to
312 assess the hardening potential of a given mine tailing material with a mafic/ultra-mafic composition.

313 Specialized software, called KITO, is being developed to simulate leaching in alkaline conditions. It
314 consists in a specific interface developed with the Scilab [57] programming language, which uses
315 PHREEQC [25] as a geochemical calculator and displays the results in pre-determined graphs. Input
316 parameters are the mineralogical composition (e.g. nature and relative amounts of minerals), the
317 NaOH concentrations, the liquid/solid ratio, and the time duration of the experiments. Some
318 minerals reactivities are limited by kinetic laws, which can optionally be taken into account in the
319 calculations. In this case, specific surface areas must also be included in the model. The precipitation
320 of secondary minerals can be predicted. Then calculations are processed according to 3 main steps:

- 321 1) Implementation of the input parameters through the KITO interface
- 322 2) Creation of the PHREEQC input file and launching of the calculations. Calculations include initial
323 equilibration, kinetic dissolution and precipitation of new minerals, if any
- 324 3) Results recovery into the KITO interface and building of the graphics.

325 A full description of KITO is given in Appendix C.

326 In this work, KITO was applied to simulate experiments described in the previous section. The
327 amounts of minerals provided by Rietveld refinement are reported in Table 8, together with the
328 surface area of the minerals. In Table 8 the weighted profile R factor R_{wp} (%) allows the Rietveld fit to
329 be assessed from the square root of the differences in intensity, scaled by the weighted

330 intensities. For most surface areas, A_{min} , reported in Table (8), the values are calculated from the
 331 mean particle diameter d , obtained by laser diffraction, considering the relation [58]:

$$332 \quad A_{min} = \frac{6.V_m}{M_m.d} \quad (7)$$

333 where V_m and M_m stand for the molar volume and the molar mass, respectively.

334 Relation (7) implies that the surface areas are approximated by their geometric value, which has
 335 been shown to be valid especially for the small-sized particles [59]. This is the case here, with $d=4.0$
 336 and $7.5 \mu\text{m}$, respectively, as mentioned earlier.

337

338

Table 8. Mine tailing analyses and surface area of the minerals

	Obenaus-Emler et al. [10]		Falah et al. [9]	
	% wt.	A_{min} ($\text{m}^2.\text{g}^{-1}$)	% wt.	A_{min} ($\text{m}^2.\text{g}^{-1}$)
Annite ⁽¹⁾	2.6	0.2	0.4	0.5
Anorthite	1.4	0.02 ⁽³⁾	2.1	0.02 ⁽³⁾
Chlorite	6.7	0.0027 ⁽²⁾	3.8	0.0027 ⁽²⁾
Calcite	2.3	0.3	4.1	0.6
Diopside	28.0	0.2	33.8	0.5
Dolomite	3.6	0.3	1.3	0.5
Forsterite	3.9	0.3	12.3	0.5
Ferro-tremolite	12.9	0.2	11.3	0.4
Enstatite	5.0	0.2	5.4	0.5
Serpentine	10.3	0.3	4.3	0.6
Magnetite	3.6	0.2	1.5	0.3
Phlogopite ⁽¹⁾	2.6	0.2	0.4	0.5
Pyrite	1.5	0.001 ⁽³⁾	1.5	0.001 ⁽³⁾
Tremolite	14.3	0.3	6.0	0.5
Quartz	1.4	0.3	1.1	0.6
Actinolite			6.4	0.5
Microcline			3.6	0.6
Albite			1.7	0.6
R_{wp} (%)	11.5		5.2	

339 (1) Annite and Phlogopite relative amounts are calculated based on the biotite amount, considering that
 340 biotite (%) = 0.5 annite (%) + 0.5 phlogopite (%)

341 (2) Chlorite surface area is fixed at $0.0027 \text{ m}^2.\text{g}^{-1}$, based on Marty et al. [13]

342 (3) Values refined from leaching experiment results

343 5. RESULTS AND DISCUSSION

344 For leaching experiments, the results of the modeling are reported in Fig. 2 which reports the
345 comparison between the modeled and the experimental values for dissolved elements. Calculation
346 results are generally in agreement with Obenaus-Emler et al. [10] experiments (Fig. 2.A and B) for
347 dissolved Si, Al, Fe, S and Ca. For the Falah et al. [9] leaching test (Fig. 2.C), the agreement is still
348 correct for Si and Al final concentrations. However, only 2 concentrations (Si and Al) were measured
349 in that case, the verification of the model is somewhat less rigorous at 25°C than at 40°C. For
350 dissolved Mg in the NaOH 10M leaching test, calculated concentrations are much lower than the
351 results from ICP analyses. It should be noted that the modified database (Table 2 and Table 3) does
352 not include a full set of Mg-OH interaction terms because of a lack in the literature. Such a gap could
353 explain why an accurate match is not reached for very high ionic strengths like in 10 M NaOH
354 solutions (Fig. 2A). In that regard, Xiong [60] and Altmaier [61] have investigated brucite ($\text{Mg}(\text{OH})_2$)
355 solubility in chloride media, for which Mg-OH specific interaction was not necessary since the
356 maximum pH value reaches 10.40 and 10.70, respectively. For the 10 M NaOH leaching, calculated
357 pH reaches 13.86, far beyond the values investigated by previous authors. Einaga [62] postulated the
358 existence of the $\text{Mg}_3(\text{OH})_4^{+2}$ complex, based on titration experiments conducted in solutions up to pH
359 11.40, at 25°C. Such pH is still too low to allow extracting relevant parameters to constrain the Mg-
360 OH interaction for our alkaline solutions. However, dissolved Mg concentrations can be correctly
361 reproduced for the 5 M NaOH leaching test, which would set the limit of ionic strength that can be
362 considered with the modified database to 5 mol.kg^{-1} . From Fig. 2A and 2B, even without specific
363 interaction terms, dissolved Fe concentrations are globally matching experimental data. However,
364 the decrease in Fe concentration after 24 hours is not correctly reproduced by the model. Modelling
365 was conducted by considering the precipitation of 2-line Ferrihydrite. Cudennec and Lecerf [63]
366 considers that this phase is the first product appearing during the oxidation of divalent iron. As the
367 oxidation process continues, the size of the coherent scattering domains would increase, leading to

368 the appearance of 6-line ferrihydrite, displaying a lower solubility ($\log_{10}K(25^\circ\text{C})$ moving from 3.40
369 (Table D1) to 3.00 [64]. The final stage would lead to hematite, with an even lower solubility [64].
370 Such evolution could explain the decrease in iron solubility which is displayed in Fig. 2.A and 2.B. The
371 transformation of 2-line ferrihydrite was not implemented in the present model, which explains why
372 the model does not correctly reproduce this tendency.

373 To account for Si decrease with time, saponite was allowed to precipitate, as a proxy of a more
374 complex silicate gel phase whose presence in the final products can only be hypothesized from the
375 evolution of the dissolved element concentration with time. In Appendix D, Fig. D1 displays an
376 example of the evolution of the relative amount of minerals. Fig. D1 corresponds to the alkaline
377 leaching by NaOH 5M solution, at 40°C, and it can be checked that ferrihydrite and especially
378 saponite precipitated amounts remain low. The corresponding dissolved element concentrations are
379 given in Fig. 2B.

380

381

382

383

384

385

386

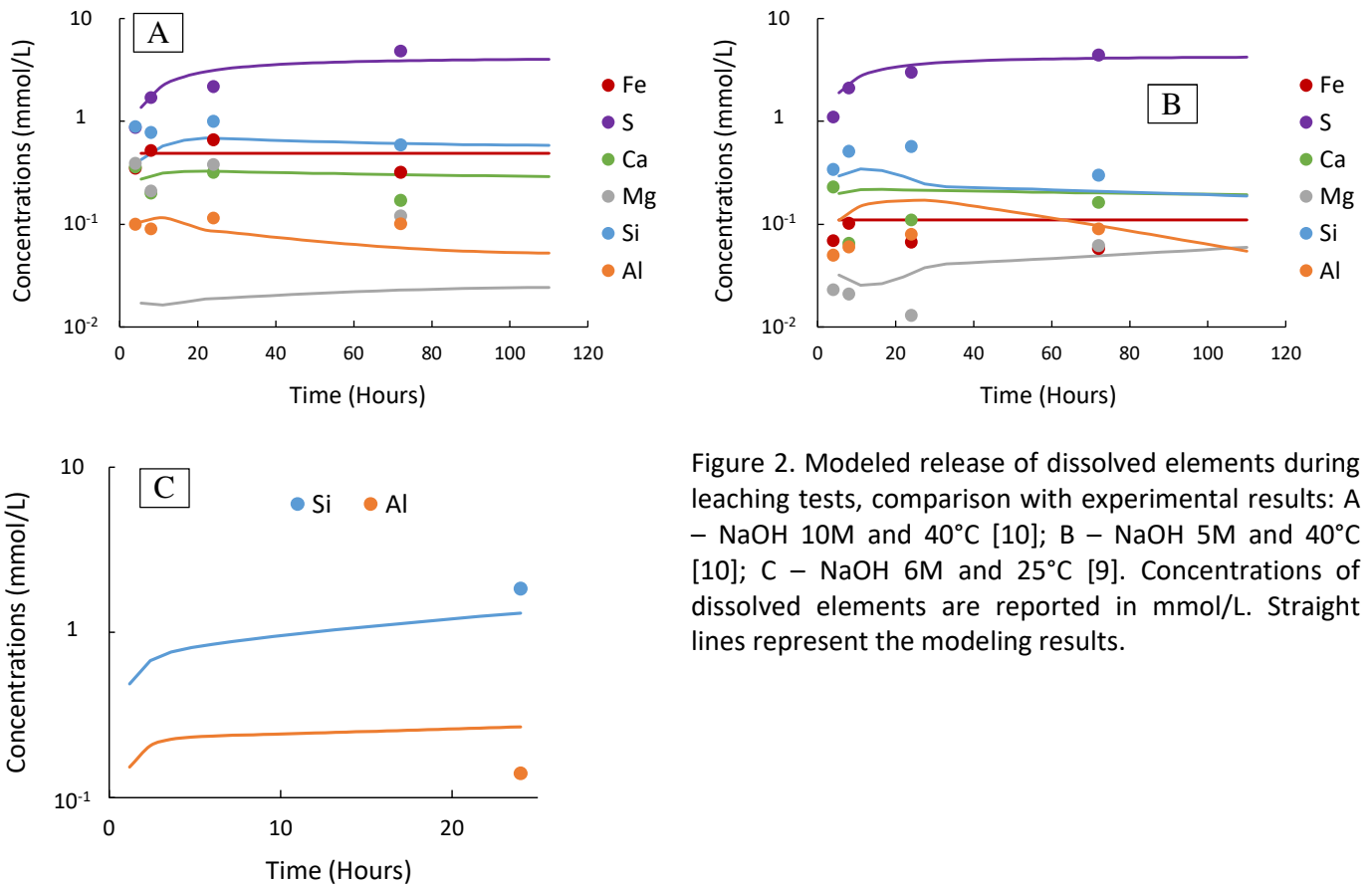
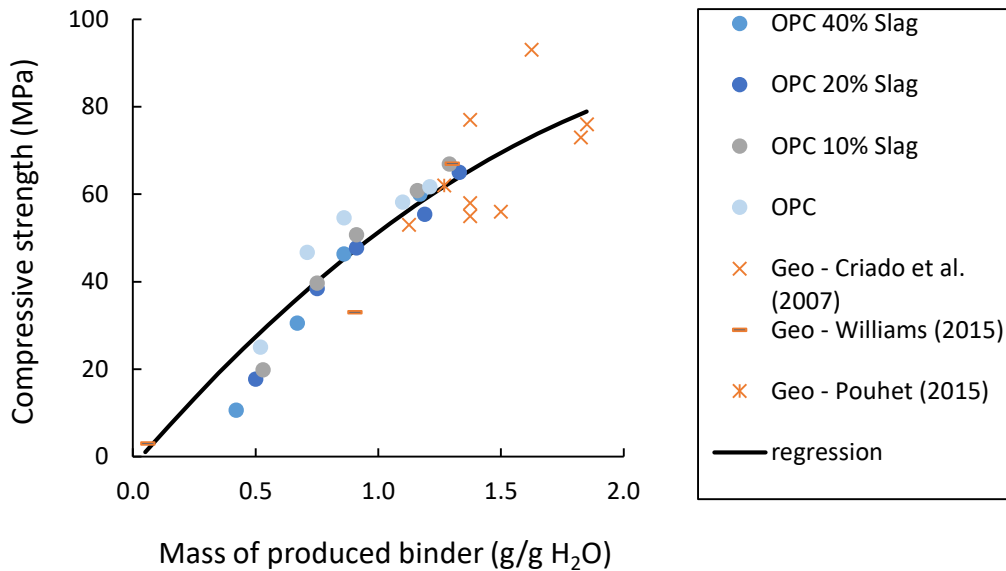


Figure 2. Modeled release of dissolved elements during leaching tests, comparison with experimental results: A – NaOH 10M and 40°C [10]; B – NaOH 5M and 40°C [10]; C – NaOH 6M and 25°C [9]. Concentrations of dissolved elements are reported in mmol/L. Straight lines represent the modeling results.

387 To reproduce the results of hardening tests, a specific treatment must be carried out since
 388 geochemical codes do not usually predict the mechanical behavior of materials. From a compilation
 389 of data from the literature, a relationship was found between the amount of hydraulic binder and
 390 the results of compressive strength tests performed on mortar. The relationship is displayed in Fig. 3
 391 in which the amount of hydraulic binder phase (HB, in g/g H₂O) produced during cement hydration is
 392 normalized to the amount of initial water and plotted vs compressive strength (CS, in MPa). A near-
 393 linear relationship is found between the sets of values ($CS = -11.33 \cdot HB^2 + 64.81 \cdot HB - 2.22$, $R^2 = 0.87$).
 394 Since the pioneering study of Powers and Brownyard [65], the relationship between porosity and
 395 compressive strength has been extensively studied in the literature and is now well established [66].
 396 However, the prediction of the porosity of a hydrating hydraulic binder powder is beyond the
 397 capacities of current geochemical codes. Instead, we can make use of an empirical relationship with
 398 the amount of hydraulic binder produced, being C-S-H or geopolymers, as reported in Fig. 3, which

399 displays the minimum amount of binder (0.022 g/g H₂O) required to obtain a compressive strength >
400 0 MPa, i.e. to achieve the setting of the hydrated powder.



401
402 Figure 3. Relationship between the mass of binder produced and mortar compressive strength test
403 results, based on literature data. OPC (Ordinary Portland Cement) data were collected from Lee et al.
404 [69]; “Geo” stands for geopolymer hardened material. Other data are collected from Criado et al.
405 [70], Williams [68] and Pouhet [67].

406
407 No literature data assessing both the amount of binder phase and the compressive strength could be
408 found for the M-S-H hydrates. However, Walling et al. [71] have demonstrated the bonding
409 capacities of M-S-H and Walling and Provis [72] do report results from refractory castables studies,
410 which demonstrates the bonding capacity of magnesia-silica based solids. For a 40% MgO/60% Silica
411 fume mixture hydrated for 28 days, Zhang et al [73] have measured compressive strengths similar or
412 slightly higher (58 MPa at W/S = 0.5) to values observed for a Portland cement by Hoshino et al. [74]
413 (52 MPa at W/S = 0.5). Very similar experiments were conducted by Tran et al. [75], which confirm
414 the similarity between M-S-H and OPC mortars, in terms of compressive strength. Lacking more
415 precise determination, we consider that the relation displayed in Fig. 3, which is based on C-S-H and
416 geopolymers, also applies for M-S-H or that the bonding capacity of M-S-H is similar to that of C-S-H.

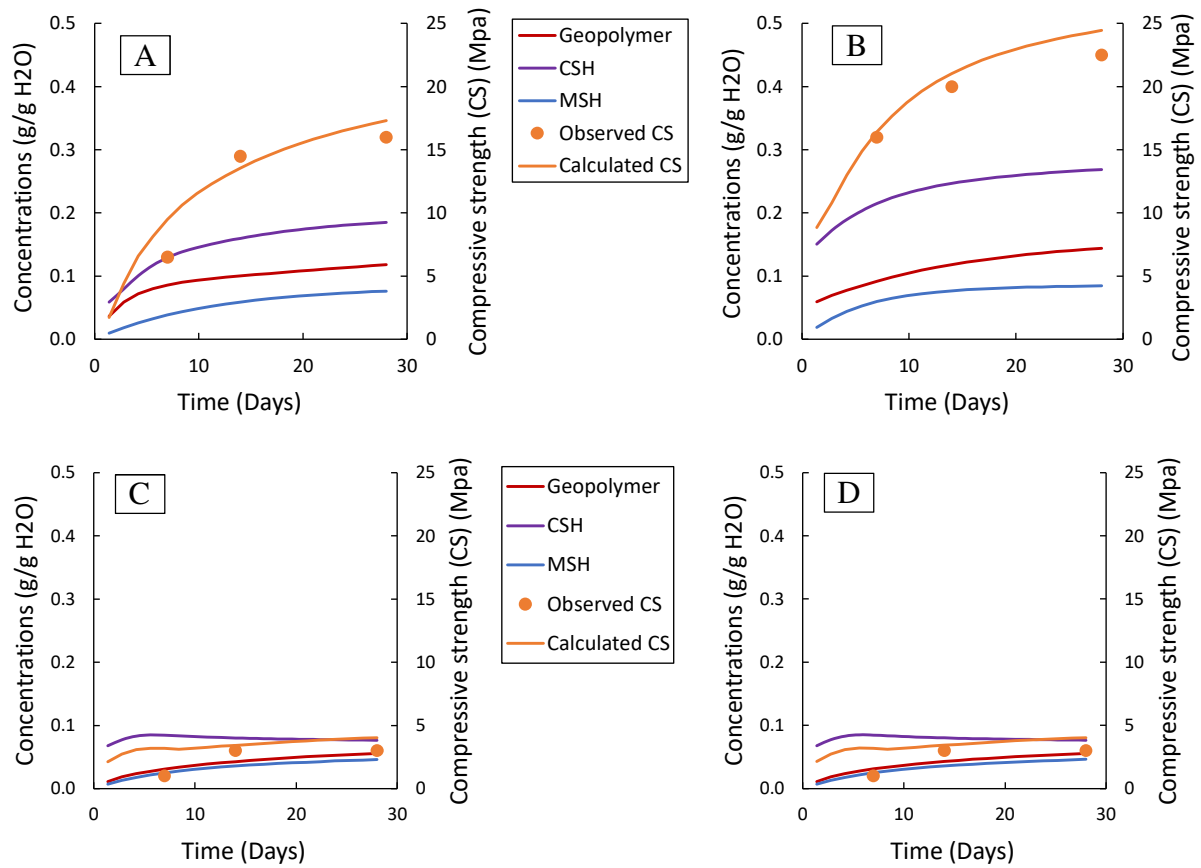
417

418

419 The modeling of the hardening tests was carried out using the database developed here, including
420 the L/S ratio, activation solution and initial mineral compositions as reported previously. Calculations
421 are reported in Fig. 4, as a function of time and compared with compressive strength test results. Fig.
422 D2 (Appendix D) displays the relative amounts of minerals, dissolved or precipitated during the
423 hydration of mine tailing activated by Na_2SiO_3 30% at 60°C. Fig. 4 includes two vertical scales, one for
424 compressive strength and one for the amount of hydraulic binder (C-S-H, M-S-H or geopolymer)
425 produced during the hardening tests. The presence of such binder phases is consistent with SEM
426 observations performed by Falah et al. [9] who detected a gel-like matrix intimately connecting
427 particles of tailings material. The authors also showed evidence of C-S-H presence, confirmed by the
428 amount of Ca and Si obtained from EDX analysis. In addition, they observed weak XRD peaks for the
429 hardened samples, which could correspond to C-S-H and M-S-H phases.

430 From this point of view, it is interesting to note that geopolymers represent only 27 to 34% of the
431 hydraulic binders produced from the geochemical calculation. This could be explained by the
432 composition of the activation solution, which is rich in silica, while the tailing samples contain about
433 15% calcium oxide. In this regard, Luukkonen et al. [52] summarized the differences observed
434 between binders obtained from alkali activation and from thermal treatment of Si- and Al-rich
435 material (specifically kaolinite clay mineral). The latter does correspond to geopolymer with a
436 predominance of Q^4 tetrahedra, while binders from alkali activation include a non-negligible
437 proportion of Q^2 [44]. Binders from alkali activation should therefore include chained silicon
438 tetrahedra, in addition to the zeolite-like 3D structure. Indeed, the calculation results indicate
439 mixtures of C-S-H and geopolymer phases, consistent with such silicate chain- and 3D silicate
440 network mixture. In our case, a mixture of zeolite-like and silica chain structure comes from a
441 mixture with different hydraulic binders rather than from a disorganization of a single binder mineral.

442



443 Figure 4. Modeled binder phases production during hardening experiments, comparison with
 444 experimental results: A – Na₂SiO₃ 30% activation at 40°C (Obenaus-Emler et al., 2019); B - Na₂SiO₃
 445 30% activation at 60°C (Obenaus-Emler et al., 2019); C - Na₂SiO₃ 10% activation at 40°C (Falah et al.,
 446 2019); D - Na₂SiO₃ 30% activation at 40°C (Falah et al., 2019). CS stands for compressive strength.

447

448 6. CONCLUSIONS

449 The geochemical modeling of alkali-activated mine tailing materials is presented here. From existing
450 databases, significant developments have been carried out, in order to account for the specific
451 interactions that take place in solutions of high ionic strengths (NaOH or Na₂SiO₃). Six dissolution rate
452 laws were either improved to account for alkaline solution or derived from literature data for
453 minerals not present in the kinetic database (Ferro-actinolite, actinolite). The database was
454 eventually supplied with a binary solid solution model, of which thermodynamic properties are
455 obtained from a polyhedral decomposition method. To facilitate the modeling of the leaching
456 experiments, a specific interface, KITO, is being developed, for use with the PHREEQC software. It
457 uses a version of the Thermoddem database which has been modified by introducing a selection of
458 Pitzer interaction coefficients. The KITO interface was used to reproduce the concentrations in
459 dissolved elements during leaching tests. The results are in good agreement with experimental
460 dissolved element concentrations, with the exception of Mg in 10 M NaOH solution, which currently
461 limits the ionic strength which can be considered in such modeling to 5 mol.kg⁻¹.

462 The modeling was finally verified with respect to compressive strength test results, by means of an
463 empirical relationship with the amount of hydraulic binder produced. Calculations suggest that, in
464 this case, the geopolymer is not the main hydraulic binder produced during the alkali activation of
465 the mine tailing samples. The resulting assemblage of C-S-H and geopolymer phases is in agreement
466 with the mixture between Q⁴ and Q² tetrahedra reported by Luukkonen et al. [52] for hardened
467 materials produced during alkali activation.

468

469

470

471

472

473

ACKNOWLEDGEMENTS

474 Financial support from the European community H2020 ITERAMS project (Grant Agreement No.
475 730480) and from the French Geological Survey (BRGM) is gratefully acknowledged. The author
476 would like to thank P. Kinnunen, as coordinator, for her friendly and efficient management of the
477 project. Many thanks to Sally Ferguson for reviewing the text. Anonymous reviewers are also
478 thanked for their decisive help in improving the manuscript.

479

480

481 **References**

482

- 483 [1] G. Orveillon, Best Available Techniques (BAT) Reference Document for the Management of Waste
484 from Extractive Industries in accordance with Directive 2006/21/EC, 2018.
- 485 [2] K. Matis, G. Gallios, K. Kydros, Separation of fines by flotation techniques, *Separations*
486 *Technology*, 3 (1993) 76-90.
- 487 [3] B.A. Wills, J. Finch, *Wills' mineral processing technology: an introduction to the practical aspects*
488 *of ore treatment and mineral recovery*, Butterworth-Heinemann 2015.
- 489 [4] J.S. Adiansyah, M. Rosano, S. Vink, G. Keir, A framework for a sustainable approach to mine
490 tailings management: disposal strategies, *Journal of Cleaner Production*, 108 (2015) 1050-1062.
- 491 [5] L.N. Bowker, D.M. Chambers, In the dark shadow of the supercycle tailings failure risk & public
492 liability reach all time highs, *Environments*, 4 (2017) 75.
- 493 [6] E. Schoenberger, Environmentally sustainable mining: The case of tailings storage facilities,
494 *Resources Policy*, 49 (2016) 119-128.
- 495 [7] T. Meggyes, E. Niederleithinger, K.J. Witt, M. Csövári, K. Kreft-Burman, J. Engels, C. McDonald, K.E.
496 Roehl, Enhancing the safety of tailings management facilities, *Soil & Sediment Contamination*,
497 17 (2008) 323-345.
- 498 [8] P.H.-M. Kinnunen, A.H. Kaksonen, Towards circular economy in mining: Opportunities and
499 bottlenecks for tailings valorization, *Journal of Cleaner Production*, 228 (2019) 153-160.
- 500 [9] M. Falah, R. Obenaus-Emler, P. Kinnunen, M. Illikainen, Effects of Activator Properties and Curing
501 Conditions on Alkali-Activation of Low-Alumina Mine Tailings, *Waste and Biomass Valorization*,
502 (2019) 1-13.
- 503 [10] R. Obenaus-Emler, M. Falah, M. Illikainen, Assessment of mine tailings as precursors for alkali-
504 activated materials for on-site applications, 2nd International Conference of Sustainable
505 Building Materials Eindhoven, The Netherlands, 2019.
- 506 [11] P. Blanc, A. Lassin, P. Piantone, M. Azaroual, N. Jacquemet, A. Fabbri, E.C. Gaucher,
507 *Thermodem: A geochemical database focused on low temperature water/rock interactions and*
508 *waste materials*, *Applied Geochemistry*, 27 (2012) 2107-2116.
- 509 [12] L. Plummer, D. Parkhurst, G. Fleming, S. Dunkle, PHRQPITZ - A Computer Program Incorporating
510 Pitzer's Equations for Calculation of Geochemical Reactions in Brines, *US Geol. Surv. Water-*
511 *Resour. Invest. Rep.*, 884153 (1988).
- 512 [13] N.C. Marty, F. Claret, A. Lassin, J. Tremosa, P. Blanc, B. Madé, E. Giffaut, B. Cochapin, C.
513 Tournassat, A database of dissolution and precipitation rates for clay-rocks minerals, *Applied*
514 *Geochemistry*, 55 (2015) 108-118.
- 515 [14] C. Roosz, P. Vieillard, P. Blanc, S. Gaboreau, H. Gailhanou, D. Braithwaite, V. Montouillout, R.
516 Denoyel, P. Henocq, B. Madé, Thermodynamic properties of C-S-H, C-A-S-H and M-S-H phases:
517 Results from direct measurements and predictive modelling, *Applied Geochemistry*, 92 (2018)
518 140-156.
- 519 [15] K.S. Pitzer, Ion interaction approach: theory and data correlation, *Activity coefficients in*
520 *electrolyte solutions*, 2 (1991) 75-153.
- 521 [16] K.S. Pitzer, Thermodynamics of electrolytes. I. Theoretical basis and general equations, *The*
522 *Journal of Physical Chemistry*, 77 (1973) 268-277.
- 523 [17] K.S. Pitzer, J.J. Kim, Thermodynamics of Electrolytes.: IV. Activity and Osmotic Coefficients for
524 Mixed Electrolytes, *Molecular Structure And Statistical Thermodynamics: Selected Papers of*
525 *Kenneth S Pitzer*, World Scientific 1993, pp. 413-419.
- 526 [18] K.S. Pitzer, G. Mayorga, Thermodynamics of electrolytes. III. Activity and osmotic coefficients for
527 2-2 electrolytes, *Journal of Solution Chemistry*, 3 (1974) 539-546.
- 528 [19] K.S. Pitzer, G. Mayorga, Thermodynamics of Electrolytes.: II. Activity and Osmotic Coefficients for
529 Strong Electrolytes with One or Both Ions Univalent, *Molecular Structure And Statistical*
530 *Thermodynamics: Selected Papers of Kenneth S Pitzer*, World Scientific 1993, pp. 396-404.

- 531 [20] J.F. Zemaitis Jr, D.M. Clark, M. Rafal, N.C. Scrivner, Handbook of aqueous electrolyte
532 thermodynamics: Theory & application, John Wiley & Sons 1986.
- 533 [21] A. Lassin, C. Christov, L. André, M. Azaroual, A thermodynamic model of aqueous electrolyte
534 solution behavior and solid-liquid equilibrium in the Li-H-Na-K-Cl-OH-H₂O system to very high
535 concentrations (40 molal) and from 0 to 250° C, American Journal of Science, 315 (2015) 204-
536 256.
- 537 [22] A. Lach, L. André, A. Lassin, M. Azaroual, J.-P. Serin, P. Cézac, A New Pitzer Parameterization for
538 the Binary NaOH-H₂O and Ternary NaOH-NaCl-H₂O and NaOH-LiOH-H₂O Systems up to
539 NaOH Solid Salt Saturation, from 273.15 to 523.15 K and at Saturated Vapor Pressure, Journal of
540 Solution Chemistry, 44 (2015) 1424-1451.
- 541 [23] A. Lassin, L. André, A. Lach, A.-L. Thadée, P. Cézac, J.-P. Serin, Solution properties and salt-
542 solution equilibria in the H-Li-Na-K-Ca-Mg-Cl-H₂O system at 25° C: A new thermodynamic model
543 based on Pitzer's equations, Calphad, 61 (2018) 126-139.
- 544 [24] A. Lach, L. André, S. Guignot, C. Christov, P. Henocq, A. Lassin, A Pitzer Parametrization To
545 Predict Solution Properties and Salt Solubility in the H-Na-K-Ca-Mg-NO₃-H₂O System at
546 298.15 K, Journal of Chemical & Engineering Data, 63 (2018) 787-800.
- 547 [25] D.L. Parkhurst, C. Appelo, Description of input and examples for PHREEQC version 3: a computer
548 program for speciation, batch-reaction, one-dimensional transport, and inverse geochemical
549 calculations, US Geological Survey, 2013.
- 550 [26] A. Lach, Modélisation thermodynamique des propriétés d'excès des saumures naturelles et
551 industrielles, 2015.
- 552 [27] C. Christov, N. Moller, Chemical equilibrium model of solution behavior and solubility in the H-
553 Na-K-OH-Cl-HSO₄-SO₄-H₂O system to high concentration and temperature, Geochimica et
554 Cosmochimica Acta, 68 (2004) 1309-1331.
- 555 [28] C. Christov, N. Moller, A chemical equilibrium of solution behavior and solubility in the H-Na-K-
556 Ca-OH-Cl-HSO₄-SO₄-H₂O system to high concentration and temperature, Geochimica et
557 Cosmochimica Acta, 68 (2004) 3717-3739.
- 558 [29] D.J. Wesolowski, D.A. Palmer, Aluminum speciation and equilibria in aqueous solution: V.
559 Gibbsite solubility at 50°C and pH 3-9 in 0.1 molal NaCl solutions (a general model for aluminum
560 speciation; analytical methods), Geochimica et Cosmochimica Acta, 58 (1994) 2947-2969.
- 561 [30] A.R. Felmy, H. Cho, J.R. Rustad, M.J. Mason, An aqueous thermodynamic model for polymerized
562 silica species to high ionic strength, Journal of Solution Chemistry, 30 (2001) 509-525.
- 563 [31] D.J. Wesolowski, Aluminum speciation and equilibria in aqueous solution: I. The solubility of
564 gibbsite in the system Na-K-Cl-OH-Al (OH)₃ from 0 to 100 C, Geochimica et Cosmochimica Acta,
565 56 (1992) 1065-1091.
- 566 [32] A.S. Russell, J.D. Edwards, C.S. Taylor, Solubility and density of hydrated aluminas in NaOH
567 solutions, JOM, 7 (1955) 1123-1128.
- 568 [33] A. Pallagi, A. Tasi, A. Gácsi, M. Csáti, I. Palinko, G. Peintler, P. Sipos, The solubility of Ca(OH)₂ in
569 extremely concentrated NaOH solutions at 25°C, Central European Journal of Chemistry, 10
570 (2011).
- 571 [34] J. Duchesne, E. Reardon, Measurement and prediction of portlandite solubility in alkali solutions,
572 Cement and Concrete Research, 25 (1995) 1043-1053.
- 573 [35] H. Konno, Y. Nanri, M. Kitamura, Crystallization of aragonite in the causticizing reaction, Powder
574 Technology, 123 (2002) 33-39.
- 575 [36] J. Schwartzentruber, W. Fürst, H. Renon, Dissolution of quartz into dilute alkaline solutions at
576 90°C: A kinetic study, Geochimica et Cosmochimica Acta, 51 (1987) 1867-1874.
- 577 [37] J.v. Lier, P.d. Bruyn, J.T.G. Overbeek, The solubility of quartz, The Journal of Physical Chemistry,
578 64 (1960) 1675-1682.
- 579 [38] I.I. Diakonov, J. Schott, F. Martin, J.-C. Harrichourry, J. Escalier, Iron (III) solubility and speciation
580 in aqueous solutions. experimental study and modelling: part 1. hematite solubility from 60 to
581 300 C in NaOH-NaCl solutions and thermodynamic properties of Fe (OH)₃-(aq), Geochimica et
582 Cosmochimica Acta, 63 (1999) 2247-2261.

- 583 [39] J.P. Greenberg, N. Møller, The prediction of mineral solubilities in natural waters: A chemical
584 equilibrium model for the Na-K-Ca-Cl-SO₄-H₂O system to high concentration from 0 to 250 C,
585 *Geochimica et Cosmochimica Acta*, 53 (1989) 2503-2518.
- 586 [40] N. Møller, The prediction of mineral solubilities in natural waters: A chemical equilibrium model
587 for the Na-Ca-Cl-SO₄-H₂O system, to high temperature and concentration, *Geochimica et*
588 *Cosmochimica Acta*, 52 (1988) 821-837.
- 589 [41] C.E. Harvie, N. Møller, J.H. Weare, The prediction of mineral solubilities in natural waters: The
590 Na-K-Mg-Ca-H-Cl-SO₄-OH-HCO₃-CO₃-CO₂-H₂O system to high ionic strengths at 25°C,
591 *Geochimica et Cosmochimica Acta*, 48 (1984) 723-751.
- 592 [42] P. Blanc, P. Vieillard, H. Gailhanou, S. Gaboreau, N. Marty, F. Claret, B. Madé, E. Giffaut,
593 ThermoChimie database developments in the framework of cement/clay interactions, *Applied*
594 *Geochemistry*, 55 (2015) 95-107.
- 595 [43] B. Lothenbach, E. Bernard, U. Mäder, Zeolite formation in the presence of cement hydrates and
596 albite, *Physics and Chemistry of the Earth, Parts A/B/C*, 99 (2017) 77-94.
- 597 [44] Y. Xiong, A thermodynamic model for silica and aluminum in alkaline solutions with high ionic
598 strength at elevated temperatures up to 100 C: Applications to zeolites, *American Mineralogist*,
599 98 (2013) 141-153.
- 600 [45] A.C. Lasaga, J.M. Soler, J. Ganor, T.E. Burch, K.L. Nagy, Chemical weathering rate laws and global
601 geochemical cycles, *Geochimica et Cosmochimica Acta*, 58 (1994) 2361-2386.
- 602 [46] J. Davidovits, Geopolymer chemistry and applications, Geopolymer Institute 2008.
- 603 [47] J.L. Provis, Alkali-activated materials, *Cement and Concrete Research*, 114 (2018) 40-48.
- 604 [48] P. Duxson, J.L. Provis, G.C. Lukey, S.W. Mallicoat, W.M. Kriven, J.S.J. van Deventer,
605 Understanding the relationship between geopolymer composition, microstructure and
606 mechanical properties, *Colloids and Surfaces A: Physicochemical and Engineering Aspects*, 269
607 (2005) 47-58.
- 608 [49] P. Duxson, A. Fernández-Jiménez, J.L. Provis, G.C. Lukey, A. Palomo, J.S.J.v. Deventer,
609 Geopolymer technology: the current state of the art, *Journal of Materials Science*, 42 (2007)
610 2917-2933.
- 611 [50] J.L. Provis, J.S.J. Van Deventer, Geopolymers: structures, processing, properties and industrial
612 applications, Elsevier 2009.
- 613 [51] J.L. Provis, S.A. Bernal, Geopolymers and Related Alkali-Activated Materials, *Annual Review of*
614 *Materials Research*, 44 (2014) 299-327.
- 615 [52] T. Luukkonen, Z. Abdollahnejad, J. Yliniemi, P. Kinnunen, M. Illikainen, One-part alkali-activated
616 materials: A review, *Cement and Concrete Research*, 103 (2018) 21-34.
- 617 [53] R.M. Hazen, A useful fiction: polyhedral modeling of mineral properties, *American Journal of*
618 *Science*, 288 (1988) 242-269.
- 619 [54] J.A. Chermak, J.D. Rimstidt, Estimating the thermodynamic properties (ΔG of and ΔH of
620) of silicate minerals at 298 K from the sum of polyhedral contributions, *American Mineralogist*,
621 74 (1989) 1023-1031.
- 622 [55] H. Helgeson, J. Delany, H. Nesbitt, D. Bird, Summary and Critique of the Thermodynamic
623 Properties of Rock-Forming Minerals, *American Journal of Science*, 278 (1978) 1-229.
- 624 [56] N. Doebelin, R. Kleeberg, Profex: a graphical user interface for the Rietveld refinement program
625 BGMN, *Journal of Applied Crystallography*, 48 (2015) 1573-1580.
- 626 [57] M. Baudin, Programming in Scilab, Scilab Consortium, (2010).
- 627 [58] B.E. Kimball, J.D. Rimstidt, S.L. Brantley, Chalcopyrite dissolution rate laws, *Applied*
628 *Geochemistry*, 25 (2010) 972-983.
- 629 [59] C. Anbeek, N. Van Breemen, E.L. Meijer, L. Van Der Plas, The dissolution of naturally weathered
630 feldspar and quartz, *Geochimica et Cosmochimica Acta*, 58 (1994) 4601-4613.
- 631 [60] Y. Xiong, Thermodynamic Properties of Brucite Determined by Solubility Studies and Their
632 Significance to Nuclear Waste Isolation, *Aquatic Geochemistry*, 14 (2008) 223-238.

- 633 [61] M. Altmaier, V. Metz, V. Neck, R. Müller, T. Fanghänel, Solid-liquid equilibria of $Mg(OH)_2(cr)$ and
634 $Mg_2(OH)_3Cl \cdot 4H_2O(cr)$ in the system Mg-Na-H-OH-Cl-H₂O at 25°C, *Geochimica et Cosmochimica*
635 *Acta*, 67 (2003) 3595-3601.
- 636 [62] H. Einaga, The hydrolytic precipitation reaction of Mg(II) from aqueous NaNO₃ solution, *Journal*
637 *of Inorganic and Nuclear Chemistry*, 43 (1981) 229-233.
- 638 [63] Y. Cudennec, A. Lecerf, The transformation of ferrihydrite into goethite or hematite, revisited,
639 *Journal of Solid State Chemistry*, 179 (2006) 716-722.
- 640 [64] J. Majzlan, A. Navrotsky, U. Schwertmann, Thermodynamics of iron oxides: Part III. Enthalpies of
641 formation and stability of ferrihydrite ($\sim Fe(OH)_3$), schwertmannite ($\sim FeO(OH)_3/4(SO_4)1/8$), and
642 $\epsilon\text{-}Fe_2O_3$ 1 1 Associate editor: D. Wesolowski, *Geochimica et Cosmochimica Acta*, 68 (2004) 1049-
643 1059.
- 644 [65] T.C. Powers, T.L. Brownyard, Studies of the physical properties of hardened Portland cement
645 paste, *Journal Proceedings*, 1946, pp. 101-132.
- 646 [66] J. Slusarek, The correlation of structure porosity and compressive strength of hardening cement
647 materials, *ARCHITECTURECIVILENGI NEERINGENV IRONMENT*, (2010).
- 648 [67] R. Pouhet, Formulation and durability of metakaolin-based geopolymers, *Université de*
649 *Toulouse, Université Toulouse III-Paul Sabatier*, 2015.
- 650 [68] R.P. Williams, Optimising geopolymer formation, *Curtin University*, 2015.
- 651 [69] H.-S. Lee, X.-Y. Wang, L.-N. Zhang, K.-T. Koh, Analysis of the optimum usage of slag for the
652 compressive strength of concrete, *Materials*, 8 (2015) 1213-1229.
- 653 [70] M. Criado, A. Fernández-Jiménez, A.G. de la Torre, M.A.G. Aranda, A. Palomo, An XRD study of
654 the effect of the SiO₂/Na₂O ratio on the alkali activation of fly ash, *Cement and Concrete*
655 *Research*, 37 (2007) 671-679.
- 656 [71] S.A. Walling, H. Kinoshita, S.A. Bernal, N.C. Collier, J.L. Provis, Structure and properties of binder
657 gels formed in the system $Mg(OH)_2\text{-}SiO_2\text{-}H_2O$ for immobilisation of Magnox sludge, *Dalton*
658 *transactions (Cambridge, England : 2003)*, 44 (2015) 8126-8137.
- 659 [72] S.A. Walling, J.L. Provis, Magnesia-Based Cements: A Journey of 150 Years, and Cements for the
660 Future?, *Chemical Reviews*, 116 (2016) 4170-4204.
- 661 [73] T. Zhang, L.J. Vandeperre, C.R. Cheeseman, Formation of magnesium silicate hydrate (MSH)
662 cement pastes using sodium hexametaphosphate, *Cement and Concrete Research*, 65 (2014) 8-
663 14.
- 664 [74] S. Hoshino, K. Yamada, H. Hirao, XRD/Rietveld analysis of the hydration and strength
665 development of slag and limestone blended cement, *Journal of Advanced Concrete Technology*,
666 4 (2006) 357-367.
- 667 [75] H. Tran, A. Scott, R. Dhakal, Strength development of mortars using a magnesium silicate
668 hydrate binder system under different curing conditions, *Academic Journal of Civil Engineering*,
669 35 (2017) 86-90.

670

Geopolymer concrete: compressive strength modeling

